Proprioceptive Control of an Over-Actuated Hexapod Robot in Unstructured Terrain

Marko Bjelonic[1], Navinda Kottege[2] and Philipp Beckerle[3]

***Abstract*— Legged robots such as hexapods have the potential to traverse unstructured terrain. This paper introduces a novel hexapod robot (Weaver) using a hierarchical controller, with the ability to efficiently traverse uneven and inclined terrain. The robot has five joints per leg and 30 degrees of freedom overall. The two redundant joints improve the locomotion of the robot by controlling the body pose and the leg orientation with respect to the ground. The impedance controller in Cartesian space reacts to unstructured terrain and thus achieves self-stabilizing behavior without prior profiling of the terrain through exteroceptive sensing. Instead of adding force sensors, the force at the foot tip is calculated by processing the current signals of the actuators. This work experimentally evaluates Weaver with the proposed controller and demonstrates that it can effectively traverse challenging terrains and high gradient slopes, reduce angular movements of the body by more than 55 % and reduce the cost of transport (up to 50 % on uneven terrain and by 85 % on a slope with 20 °). The controller also enables Weaver to walk up inclines of up to 30 °, and remain statically stable on inclines up to 50 °. Furthermore, we present a new metric for legged robot stability performance along with a method for proprioceptive terrain characterization.**

I. INTRODUCTION

Locomotion of wheeled robots is limited by extreme terrain. In contrast, legged robots have the potential to overcome this by adapting their gaits [1]. The advantage of hexapods compared to bipeds or quadrupeds is the static stability during walking [2]. The stability and the range of available gait patterns increase with the number of legs. The largest improvement is from four to six legs. For legged robots with more than six legs the improvement becomes significantly smaller and the hardware cost increases [3].

When traversing rough terrain, it is crucial to control the stability of the robot. One approach is to feedback the state of the body to the controller and to adapt the leg positions [4], [5]. However, additional sensors are needed for such body regulation. Biological investigation reveals that locomotion of running and bouncing animals can be described by a spring attached to a mass [6] and that an elastic leg configuration achieves self-stabilization [7]. Self-stabilizing refers to stable locomotion without feedback of the body dynamics by additional sensors [8]. The challenge of robots with flexible joints is the time-varying displacement between motor and link position. Without specific control algorithms, oscillatory behavior and instability may occur during ground contact [9]. Additional position encoders at the driven links increase the hardware cost. The MIT Cheetah [8] and the COMET-IV [10] propose a virtual leg compliance instead of adding elastic behavior to the mechanical system. Building upon this work, this paper introduces a low-level controller with virtual second order mechanical characteristics implemented on a novel hexapod robot platform named Weaver (Fig. 1). The current of the motors are translated into forces at the foot tips and the forces are further processed by an impedance controller in Cartesian space. This controller introduces:

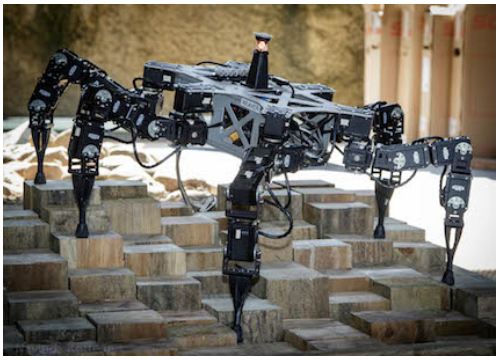

Fig. 1. Weaver on the multi-terrain testbed.

- Reactive leg control on unstructured terrain without prior profiling of the environment.
- Self-stabilizing and energy efficient locomotion by maintaining ground contact.
- Terrain characterization using foot tip positions.

Many of the developed hexapods are using insect-inspired three degrees of freedom (DoF) per leg. Legged robots like Messor-II, AMOS II, DLR-Crawler and BILL-Stick [11]–[14] are only able to control the position of the foot tip. The LAURON V [15] and ASTERISK [16] robot have four independent joints. In [15] the authors show how the fourth rotational joint in the bio-inspired leg kinematics improves the maneuverability of the robot by controlling the orientation of the leg in longitudinal direction. On steep slopes the LAURON V robot decreases the torque and increases the stability of the robot. The robot introduced in this paper, Weaver has five joints per leg and this enables it to control the position and orientation of the leg. In contrast to LAURON V, Weaver copes with high gradient slopes in any orientation, not only in longitudinal direction. An inclination controller specifies the desired orientation of the leg and adapts the body pose. The novel leg configuration of

[1] M. Bjelonic is a student at the Faculty of Mechanical Engineering, Technische Universität Darmstadt, 64287 Darmstadt, Germany and was with the Autonomous Systems Lab, CSIRO, Pullenvale, Brisbane, QLD 4069, Australia at the time of this study.

[2] N. Kottege is with the Autonomous Systems Lab, CSIRO, Pullenvale, Brisbane, QLD 4069, Australia. Correspondance should be addressed to navinda.kottege@csiro.au

[3] P. Beckerle is with the Institute for Mechatronic Systems in Mechanical Engineering, Technische Universität Darmstadt, 64287 Darmstadt, Germany

Weaver and the inclination controller contribute to efficient locomotion, increased maneuverability and stability on steep inclines.

The rest of the paper is organized as follows: Forward and inverse kinematics are presented in Section II, the inclination and impedance controller are introduced in Section III, Section IV describes the experimental setup and shows the results from the experiments. Section V discusses the results and Section VI concludes the paper with insights for extensions.

II. KINEMATICS

The overall configuration of Weaver with 30 DoF is shown in Fig. 2. Each leg of the robot uses a yaw-roll-pitch-pitch-pitch kinematic design. The naming convention of the joints of each leg corresponds to the attached link name and the structure of the leg is further illustrated in Fig. 3.

The transformation in Fig. 2 from world frame $(o_0x_0y_0z_0)$ to body frame $(o_1x_1y_1z_1)$ takes into account the body's travelled distances x, y and z, and rotations q_{roll}, q_{pitch} and q_{yaw}. The calculation of the inverse kinematics is performed once for each leg. In order to use the same frame for each leg, the body frame $(o_1x_1y_1z_1)$ is transformed to the leg frame (or Coxa frame) $(o_2x_2y_2z_2)$. Fig. 2 shows the relationship between these frames for Leg 2 (middle-left leg).

A. Forward Kinematics

The forward kinematics of the leg is based on the Denavit-Hartenberg (DH) convention. The five joint angles of each leg in Fig. 3 are denoted by q_1, q_2, q_3, q_4 and q_5. The DH convention uses the following homogeneous transformation:

$$H^i_{i+1} = Rot_{z,\theta_i} \cdot Trans_{z,d_i} \cdot Trans_{x,a_i} \cdot Rot_{x,\alpha_i} = \begin{bmatrix} c_{\theta_i} & -s_{\theta_i}c_{\alpha_i} & s_{\theta_i}s_{\alpha_i} & a_ic_{\theta_i} \\ s_{\theta_i} & c_{\theta_i}c_{\alpha_i} & -c_{\theta_i}s_{\alpha_i} & a_is_{\theta_i} \\ 0 & s_{\alpha_i} & c_{\alpha_i} & d_i \\ 0 & 0 & 0 & 1 \end{bmatrix} \quad (1)$$

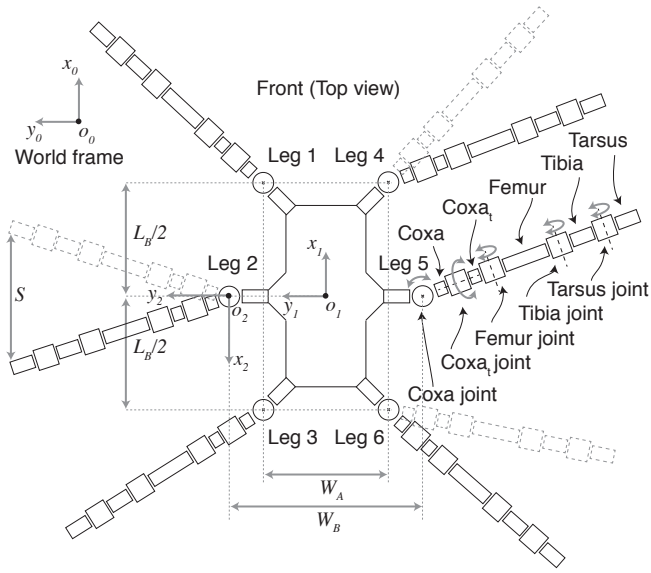

Fig. 2. Structure and body dimensions of the 30 DoF hexapod.

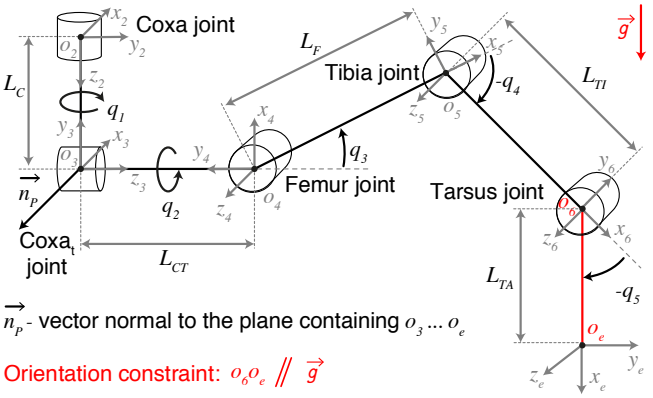

Fig. 3. Structure of the 5 DoF leg (yaw-roll-pitch-pitch-pitch).

where c_x and s_x denote $\cos(x)$ and $\sin(x)$ respectively. The superscript in the notation of H^j_i denotes the reference frame $(o_jx_jy_jz_j)$ and the subscript indicates the transformed frame $(o_ix_iy_iz_i)$. The DH parameters θ_i, d_i, a_i and α_i are the rotation around z, translation along z, translation along x and rotation around x, respectively. The transformation from Coxa frame to end effector frame is

$$H^2_e = H^2_3(q_1) \cdot H^3_4(q_2) \cdot H^4_5(q_3) \cdot H^5_6(q_4) \cdot H^6_e(q_5) \quad (2)$$

The coordinates of the foot tip p_{e2} with respect to frame $(o_2x_2y_2z_2)$ are given by the first three elements of the fourth column of H^2_e. Table I lists DH parameters for a given leg to be substituted in (2).

The force vector $F^2_e = [F_x \ F_y \ F_z]^T$ and the torque vector $M^2_e = [M_x \ M_y \ M_z]^T$ at the foot tip with respect to frame $(o_2x_2y_2z_2)$ are obtained through the static wrench transmission using the Jacobian J_e and the joint torques $M_q = [M_1 \ M_2 \ M_3 \ M_4 \ M_5]^T$.

$$\begin{bmatrix} F^2_e(t) \\ M^2_e(t) \end{bmatrix} = (J_e(q_1, q_2, q_3, q_4, q_5)^T)^{-1} \cdot M_q \quad (3)$$

B. Inverse Kinematics

The given robot configuration is redundant since the five DoF of each leg are only constrained by a three dimensional *position* of the foot tip. In order to find a closed form solution, the leg is additionally constrained by a desired foot tip *orientation*. The control angles δ_d and β_d in Fig. 4 constrain the orientation of the legs. Both angles fully describe the orientation of the gravity vector $\vec{g}$ relative to the Coxa frame $(o_2x_2y_2z_2)$. The first constraint angle δ_d defines the rotation around the y_2 axis and the second angle β_d rotates around the current x'_2 axis. The inclination

TABLE I
DENAVIT-HARTENBERG PARAMETERS FOR A GIVEN LEG.

Link	θ_i	d_i	α_i	a_i
Coxa	q_1	L_C	$-\pi/2$	0
Coxa$_t$	$q_2 + \pi/2$	L_{CT}	$-\pi/2$	0
Femur	$q_3 - \pi/2$	0	0	L_F
Tibia	q_4	0	0	L_{TI}
Tarsus	q_5	0	0	L_{TA}

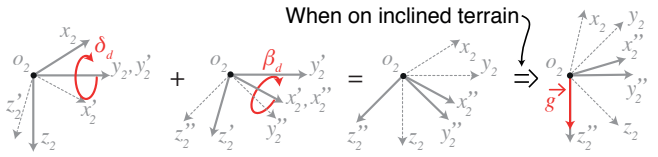

Fig. 4. Control angles δ_d and β_d describe the orientation of the gravity vector $\vec{g}$ relative to the leg frame (or Coxa frame).

control algorithm in Section III determines these control angles and the following inverse kinematics aligns the Tarsus link (o_6o_e) with the gravity vector $\vec{g}$ (Figs. 3, 4). The additional constraint improves the locomotion in terms of speed and energy efficiency when traversing an inclination by aligning the legs parallel to the gravity vector [15]. As previously discussed, LAURON V robot is compensating for inclinations by controlling only δ_d to align the last link with $\vec{g}$ [17]. This means it can only handle gradients along the longitudinal axis. Weaver can compensate for inclinations by aligning the Tarsus link with $\vec{g}$ at an arbitrary body orientation by having control over both δ_d and β_d.

Geometric observations reveal that all joints lower than the $\mathrm{Coxa_t}$ joint are on the same plane. The normal vector of the plane is obtained from the DH transformation and becomes

$$\vec{n}_p = [-c_1 \cdot c_2, -s_1 \cdot c_2, s_2]^T \tag{4}$$

in which c_i and s_i denote $\cos(q_i)$ and $\sin(q_i)$ respectively. The equation of this plane is given by

$$-c_1 \cdot c_2 \cdot x_2 - s_1 \cdot c_2 \cdot y_2 + s_2 \cdot (z_2 - L_C) = 0 \tag{5}$$

The first two joint angles q_1 and q_2 fully define the orientation of the leg. By inserting the desired foot tip position (x_{d2}, y_{d2}, z_{d2}) relative to the Coxa frame $(o_2x_2y_2z_2)$ and the desired position of the Tarsus joint $(x_{d2,TA}, y_{d2,TA}, z_{d2,TA})$ into (5), we obtain two equations for the two unknown angles q_1 and q_2:

$$q_1 = \arctan\left(\frac{a_1(z_{d2} - L_C) - x_{d2}}{y_{d2} - a_2(z_{d2} - L_C)}\right) \tag{6}$$

$$q_2 = \arctan\left(a_1 \cos(q_1) + a_2 \sin(q_1)\right) \tag{7}$$

where

$$a_1 = \frac{(\sin(\delta_d)\cos(\beta_d) - b_1 \sin(\beta_d) b_2 L_{TA}}{-\cos(\delta_d)\cos(\beta_d) L_{TA} - L_C} \tag{8}$$

$$a_2 = \frac{(\sin(\beta_d + b_1 \sin(\delta_d)\cos(\beta_d)) b_2 L_{TA}}{-\cos(\delta_d)\cos(\beta_d) L_{TA} - L_C} \tag{9}$$

and the desired position of the Tarsus joint is

$$\begin{aligned} x_{d2,TA} &= x_{d2} + (\sin(\delta_d)\cos(\beta_d) - b_1 \sin(\beta_d) b_2 L_{TA} \\ y_{d2,TA} &= y_{d2} + (\sin(\beta_d + b_1 \sin(\delta_d)\cos(\beta_d)) b_2 L_{TA} \\ z_{d2,TA} &= z_{d2} - \cos(\delta_d)\cos(\beta_d) L_{TA} \end{aligned} \tag{10}$$

The parameters b_1 and b_2 change between front ($b_1 = 1$, $b_2 = \sqrt{2}/2$), middle ($b_1 = 0$, $b_2 = 1$) and rear legs ($b_1 = -1$, $b_2 = \sqrt{2}/2$) because the front and rear Coxa frames are rotated by 45 °and -45 °respectively (Fig. 2).

What remains of the inverse kinematics is the positioning of the last three joints within the plane. Fig. 5 shows the remaining three joints and their geometrical dependencies. First, the desired position of the foot tip (x_{d2}, y_{d2}, z_{d2}) and the desired position of the Tarsus joint (10) are transformed from the frame $(o_2x_2o_2y_2z_2)$ to the frame $(o_4x_4o_4y_4z_4)$. This is equivalent to the inverse of the homogeneous transformation described by $H_4^2(q_1, q_2)$. Due to these joints being on a plane, the z coordinates are all considered to be zero and will not be included in the following equations. The desired position of the foot tip (x_{d4}, y_{d4}) and Tarsus joint $(x_{d4,TA}, y_{d4,TA})$ relative to the Femur frame set the joint angle q_5 to

$$q_5 = -\arctan\left(\frac{x_{d4,TA} - x_{d4}}{y_{d4,TA} - y_{d4}}\right) - q_3 - q_4 \tag{11}$$

The vector sum of the triangle between the Femur and Tibia link gives

$$q_4 = \arctan(\pm\sqrt{1 - D^2}/D) \tag{12}$$

where

$$D = \frac{(x_{d4,TA})^2 + (y_{d4,TA})^2 - L_F^2 - L_{TI}^2}{2 L_F L_{TI}} \tag{13}$$

The two solutions of q_4 correspond to "Tibia up" and "Tibia down" configurations. The remaining joint angle q_3 is derived by subtracting the angles in the triangle:

$$q_3 = -\arctan\left(\frac{x_{d4,TA}}{y_{d4,TA}}\right) - \arctan\left(\frac{L_{TI} s_4}{L_F + L_{TI} c_4}\right) \tag{14}$$

The function $atan2()$ is used to return the angle of the appropriate quadrant and to avoid divisions by zero.

III. ROBOT CONTROL

The hierarchical control architecture of Weaver contains a low-level and high-level part. Our main contributions stem from the low-level controller and the inclination controller which improves locomotion on rough terrain as well as inclined terrain. Fig. 6 shows the control architecture of the robot and Table II describes the signals. The commands from the operator are translated into a desired body pose and body velocity relative to the world frame $(o_0x_0y_0z_0)$.

The hexapod moves by coordinating the movement of its six legs. The "stance phase" and the "swing phase" describe

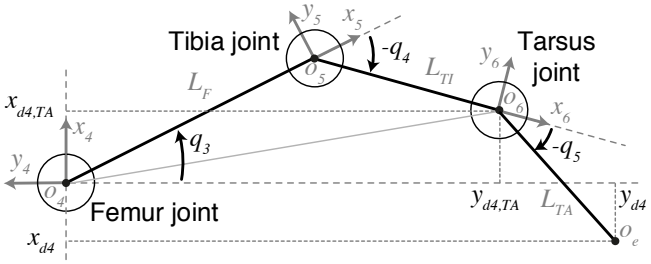

Fig. 5. Configuration of the Femur, Tibia and Tarsus joints on a plane.

TABLE II

SIGNAL DESCRIPTION OF THE HIERARCHICAL CONTROLLER.

Signals	Symbols	SI units
Pitch and roll angle	$[q_{pitch}, q_{roll}]$	rad
Foot positions	$[p_1, p_2, p_3, p_4, p_5, p_6]$	m
Desired body pose	$[\Delta o_1, q_{pitch,d}, q_{roll,d}]$	m,rad
Delta foot trajectory	$[\Delta x_{r2}, \Delta y_{r2}, \Delta z_{r2}]$	m
Foot trajectory	$[x_{r2}, y_{r2}, z_{r2}]$	m
Des. foot trajectory	$[x_{d2}, y_{d2}, z_{d2}]$	m
Des. motor positions	$[q_{d1}, q_{d2}, q_{d3}, q_{d4}, q_{d5}]$	rad
PID signals	$[I_1, I_2, I_3, I_4, I_5]$	A
Motor positions	$[q_1, q_2, q_3, q_4, q_5]$	rad
Motor torques	$[M_1, M_2, M_3, M_4, M_5]$	Nm
Force at the foot	$[F_x, F_y, F_z]$	N

that the leg is in contact with the ground and that the leg swings in a certain direction, respectively. A "stride" is the combination of both movements and by repeating the execution of strides the robot performs a gait. By performing different sequences of stance and swing phases the robot moves with different gait patterns. In this context, the duty factor β is the ratio between the durations each leg spends in stance phase T_{Stance} and stride phase T_{Stride}. The "wave" and the "tripod" gait are typical gaits for hexapod robots. The wave gait has one leg in swing phase and all other five legs in stance phase ($\beta = 5/6$) and the tripod gait has three legs in swing phase and three legs in stance phase ($\beta = 3/6$) [18], [19].

The foot path planner generates a foot trajectory for each leg. The swing phase is modelled by a Bézier curve. An important parameter is the length of the stride S shown in Fig. 2. While the stride frequency stays constant, body velocity increases with increasing stride length.

A. Inclination Control

The inclination controller in Fig. 6 determines the orientation of the gravity vector relative to the body frame and increases the stability by shifting the center of mass (CoM). The orientation of the gravity vector relative to the Coxa frame $(o_2 x_2 y_2 z_2)$ can be defined using the two control angles δ_d and β_d in Fig. 4. In combination with the inverse kinematics the inclination controller aligns the force ellipsoid of the foot tip with the gravity vector. This increases energy efficiency and maneuverability when traversing inclinations

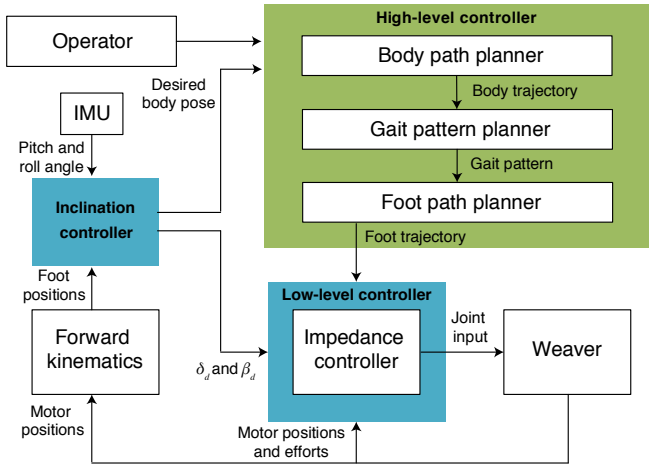

Fig. 6. The hierarchical control architecture of Weaver.

because the gravitational force is supported with least amount of effort [13]. Furthermore, the inclination controller sets the body pose to increase the Normalized Energy Stability Margin (NESM). The NESM is a stability criteria for walking robots on rough terrain and it is defined as the difference between the robot's maximum and initial potential energy normalized by weight [20]. A desired pitch angle $q_{pitch,d}$ and roll angle $q_{roll,d}$ of the body, and the translation of the body shifts the CoM to a stable body pose.

An inertial measurement unit (IMU) measures the pitch q_{pitch} and roll angle q_{roll} of the robot, and the current inclination angles of the ground relative to the body are calculated by

$$[q_{inc,p}, q_{inc,r}] = [f(q_{pitch}, P_i), f(q_{roll}, P_i)] \tag{15}$$

where the angles $q_{inc,p}$ and $q_{inc,r}$ denote the part of the inclination gradient in pitch and roll direction of the body, respectively. P_i is the set of the six foot tip positions. The desired pitch $q_{pitch,d}$ and roll angle $q_{roll,d}$ of the body are proportional to the current inclination.

$$[q_{pitch,d}, q_{roll,d}] = [k_{p,1} \cdot q_{inc,p}, k_{r,1} \cdot q_{inc,r}] \tag{16}$$

in which the constant values $k_{p,1} \in [0,1]$ and $k_{r,1} \in [0,1]$ reduce the desired body angles to keep the leg inside of its workspace [21]. The translation of the body centre $\Delta o_1 = [\Delta x_1, \Delta y_1, \Delta z_1)]^T$ is

$$\begin{bmatrix} \Delta x_1 \\ \Delta y_1 \\ \Delta z_1 \end{bmatrix} = Rot_{q_{rot,p},y_2} Rot_{q_{rot,r},x_2} \begin{bmatrix} 0 \\ 0 \\ z_{body} \end{bmatrix} - \begin{bmatrix} 0 \\ 0 \\ z_{body} \end{bmatrix} \tag{17}$$

where

$$[q_{rot,p}, q_{rot,r}] = [k_{p,2} \cdot q_{inc,p}, k_{r,2} \cdot q_{inc,r}] \tag{18}$$

with $k_{p,2} \in [0,1]$ and $k_{r,2} \in [0,1]$. $Rot_{q_{rot,p},y_2}$ and $Rot_{q_{rot,r},x_2}$ define the rotation matrix around the y_2 axis and x_2 axis, respectively. The value z_{body} is the body height

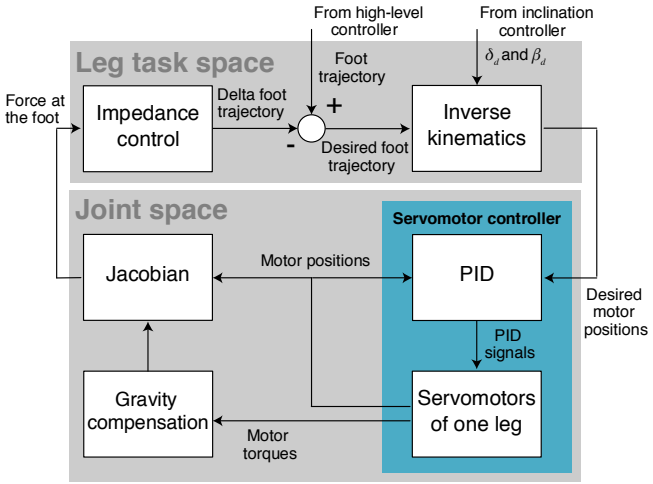

Fig. 7. Block diagram describing the low-level controller for one leg with five joints. In joint space, signals are treated as SISO for the five joints of each leg. The task space contains the foot trajectory of one leg.

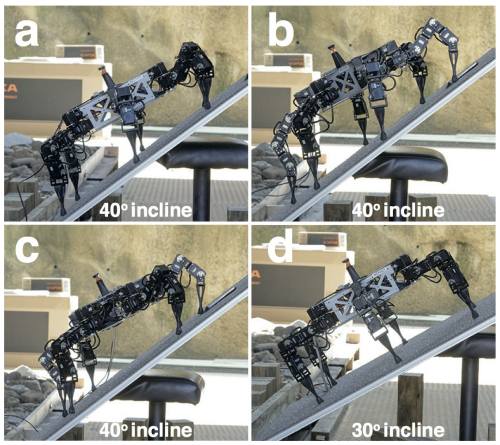

Fig. 8. Inclination controller in combination with the inverse kinematics: Inclination in longitudinal (a), longitudinal and transverse (b), transverse (c) direction with respect to the body frame's x_1 axis and with inclination control off (d).

above ground. Finally, the output of the inclination controller or respectively the input of the inverse kinematics is

$$[\delta_d, \beta_d] = [(1 - k_{p,1}) \cdot q_{inc,p}, (1 - k_{r,1}) \cdot q_{inc,r}] \tag{19}$$

Fig. 8 shows the effect of the inclination controller in combination with the inverse kinematics.

B. Low-Level Control

When traversing uneven terrain it is crucial to control the contact between the foot tip and ground. With force control it is possible to add virtual elastic elements to a mechanically stiff configuration such that on uneven terrain, the legs adapt to maintain ground contact. Impedance control is one approach of indirect force control and achieves the desired dynamic behavior of the legs. A second order mechanical system consists of a mass, damper and spring [22]. The impedance controller design in Fig. 7 with the description in Table II does not require inverse dynamics with state feedback to linearize the mechanical system. The only requirements are the inverse kinematics and the force at the foot tip. This makes the controller versatile for any legged robot with arbitrary joint configurations.

The impedance controller in Cartesian space transforms the force at the foot tip into a resulting position. A virtual mass m_{virt}, virtual stiffness c_{virt} and virtual damping element b_{virt} define the dynamic behavior in the z_2 direction. The natural frequency $\omega_0^2 = c_{virt}/m_{virt}$ and the damping ratio $D = b_{virt}/(2\sqrt{m_{virt}c_{virt}})$ are useful parameters to describe the second order system given by

$$-\frac{F_z}{m_{virt}} = \Delta\ddot{z}_{r2} + 2D\omega_0\Delta\dot{z}_{r2} + \omega_0^2\Delta z_{r2} \tag{20}$$

The damping ratio D sets the behavior in terms of undamped ($D = 0$), underdamped ($D < 1$), overdamped ($D > 1$) and critically damped ($D = 1$).

The virtual second order mechanical system reacts on ground reaction forces and adapts the desired foot trajectory. The positions Δx_{r2} and Δy_{r2} are set to zero in order to keep the stiff behavior of the leg in x_2 and y_2 direction. The adapted leg position becomes

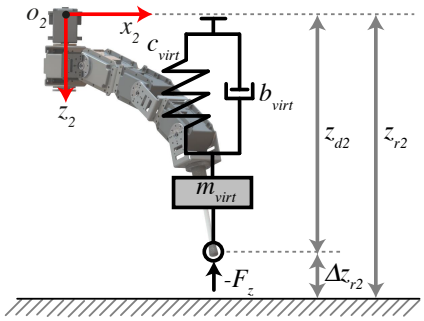

Fig. 9. The equivalent model of the impedance controller is a second order mechanical system attached to the foot tip.

$$[x_{d2}, y_{d2}, z_{d2}]^T = [x_{r2}, y_{r2}, z_{r2} - \Delta z_{r2}]^T \tag{21}$$

The equivalent model of (20) and (21) is shown in Fig. 9. Weaver's mass causes pre-stressing of the virtual dynamic elements in (20). Hence, the induced torques at each link are canceled by the gravity compensation. The impedance controller only uses the force in z_2 direction and the force $|F_t| = (F_x^2 + F_y^2)^{1/2}$ is used to detect obstacles. If the force is greater than a tuned heuristic threshold, the stride height of the foot tip increases.

The desired and current motor positions of the five joints are processed by a PID controller. Each joint is controlled as as single-input single-output system (SISO) and coupling effects are treated as disturbances. The main objectives of the independent joint controller are trajectory tracking and disturbance rejection.

IV. EXPERIMENTS AND RESULTS

The following section shows the criteria that are used to evaluate Weaver's performance.

A. Performance Criteria

The dimensionless energetic cost of transport (CoT) is a popular performance indicator in the wheeled and legged robotics communities used to compare performance of different robots [18], [23]. It is defined as

$$CoT = UI/(mgv) \tag{22}$$

where U is the voltage of the power supply, I is the instantaneous current drawn from the power supply, m is the mass and v is the velocity of the robot. The estimated power consumption $P \approx UI$ consists of the mechanical power of the motors, heat dissipated by the robot and other losses like friction. Thus, the overall power consumption P highly depends on the motor characteristics but this is not considered in this work.

Uneven terrain causes undesirable movement in pitch and roll. The self-stabilizing effect of the impedance controller minimizes the angular movements. The percentage reduction of variance S_i is a novel stability criteria for legged robot and comes from ship control assessment [24]:

$$S_i = 100 \cdot \left(1 - \frac{Var(X_{i,imp})}{Var(X_{i,u})}\right) \quad (23)$$

where i is a place holder for the movement in pitch and roll. The function $Var()$ is the variance and the variable X_i is the set of observed values in radian. The subscripts imp and u stand for impedance and unstabilized, respectively.

Weaver adapts its legs on uneven terrain to maintain ground contact. It is possible to estimate the center line average [25] of the roughness R_a by processing the difference of the six foot tip positions in z direction using forward kinematics.

B. Experimental Setup

In all experiments Weaver had no information about its environment and no exteroceptive sensors were used. A human operator controlled the robot via joystick (via velocity commands) and the tripod gait was used. During experimentation, the velocity v of the robot was tracked at 4 Hz using a robotic total station (Leica TS12) with a target prism mounted on the robot. The power consumption P was measured at 20 Hz by an Arduino based system sensor. The torque from the servomotors of Weaver is an unknown function of the servomotor's current and it is modeled as a linear function ($M_i = k_C I_i$). This estimation neglects large friction losses and the constant calibration gains k_C were determined in a separate experiment with an ATI Mini45 Force/Torque sensor. A fourth order Runge-Kutta solver was solving (20) and the parameters of the impedance controller were $c_{virt} = 1044\,\mathrm{Nm}^{-1}$, $\omega_0 = 0.89\,\mathrm{s}^{-1}$ and $D = 0.7$. In the inclination controller the parameters were set to $k_{p,1} = k_{r,1} = 0.35$ and $k_{p,2} = k_{r,2} = 0.75$. Table III lists the specifications of Weaver.

The following results compare the behavior of standard position control with the above described impedance and inclination controllers. The experiments are divided into three parts. The first part is on flat terrain and the second part is a plane with different inclination angles. The contact surface of the inclination consists of a carpet surface and the robot has rubber feet. The third part is on the multi-terrain testbed in Fig. 10 which evaluates the performance of Weaver

TABLE III

SPECIFICATIONS OF WEAVER.

Type	Description
General	$m = 7.03\,\mathrm{kg}$; Body dimensions: $L_B = 0.35\,\mathrm{m}$, $W_A = 0.18\,\mathrm{m}$, $W_B = 0.28\,\mathrm{m}$; Leg dimensions: $L_C = 0.0665\,\mathrm{m}$, $L_{CT} = 0.062\,\mathrm{m}$, $L_F = 0.1065\,\mathrm{m}$, $L_{TI} = 0.088\,\mathrm{m}$, $L_{TA} = 0.135\,\mathrm{m}$ (See Figs. 2,3)
Servomotors	Dynamixel MX-64 (Coxa, Tibia, Tarsus) with torque calibration gain $k_C = 16.06$ and Dynamixel MX-106 ($\mathrm{Coxa_t}$, Femur) with torque calibration gain $k_C = 22.22$ (38 Hz)
Power supply	2× 4-cell LiPo batteries (14.8 V, 4000 mAh each)
On-board PC	Intel NUC mini PC (Intel Core i5 processor, 16 GB RAM) running Robot Operation System (ROS) in an Ubuntu environment
Sensors	Microstrain GX3 IMU (100 Hz)

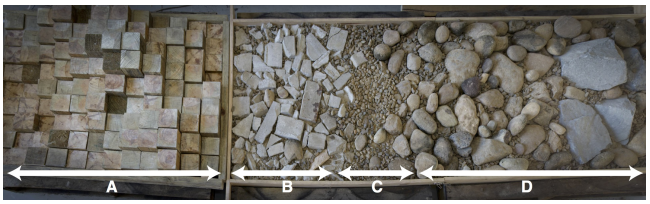

Fig. 10. Multi-terrain testbed with maximum height difference: 113 % (A), 28 % (B), 11 % (C) and 72 % (D) of Weaver's body height.

on uneven terrain. Segment A of the testbed contains wooden blocks of various heights and segment B-C-D is a mixture of sand, pebbles, river stones, crumbled concrete and bigger stones. Besides the uneven ground condition, the challenging part of the testbed is the inclination gradient. The robot faces inclination angles in different directions with respect to the body's x_1 axis and thus, the inclination control needs to adapt both control angles (δ_d and β_d) of the inverse kinematics.

C. Results

The first experiment evaluates the performance on flat terrain. The flat-terrain experiment was repeated three times for each controller and the results are summarized in Table IV. The impedance controller has a slightly higher CoT on flat terrain. Investigations revealed that the virtual compliance induces additional movement of the legs due to impact forces.

The second experiment evaluates the performance on high gradient slopes. Fig. 11 shows Weaver on different inclination angles and the results in Table V shows the CoT of both controllers. The impedance and inclination controller has a distinctly lower CoT compared to the position controller without inclination control and it increases the maximum inclination angle significantly. This result comes clearly from the improved leg configuration of the inclination controller using the proposed inverse kinematics. The percentage reduction of CoT on a 20° inclination is $85.1\,\%$. Weaver walks up inclinations up to 30 °and remains static stable until 50 °. Without inclination control the robot walks up inclinations up to 20 °and remains static stable until 30 °. The reasons for failing are slipping at the foot tip and reaching the torque limits of the actuators.

The multi-terrain testbed in Fig. 10 evaluates the performance of Weaver on uneven terrain. Fig. 12 shows the mean (black line) and standard deviation (grey shading) of the CoT from 15 runs with the impedance and inclination controller. Two runs are showing the CoT of the position controller (blue and red line). The proprioceptive roughness estimate R_a (green line) is based on 15 runs with the impedance and inclination controller. It is calculated by processing the

TABLE IV

RESULTS OF THE FLAT-TERRAIN EXPERIMENT.

Controller	Power in W	Velocity in ms^{-1}	CoT
Position control	124.2 ± 8.5	0.119 ± 0.0051	15.2 ± 1.25
Impedance control	132.4 ± 9.5	0.103 ± 0.0035	18.1 ± 1.61

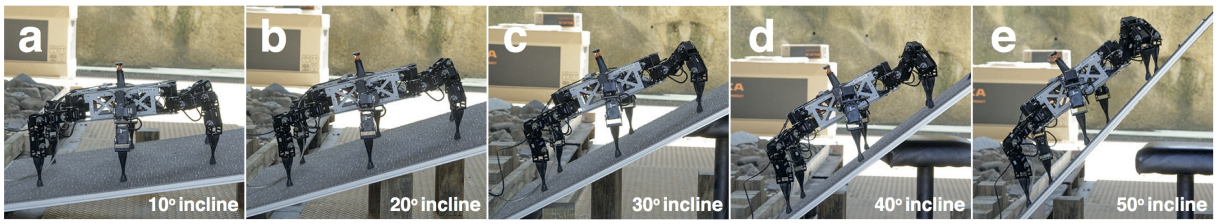

Fig. 11. Inclination control test.

TABLE V
RESULTS OF THE INCLINATION EXPERIMENT (WALKING UP).

Inclination angle	CoT of position control only	CoT of impedance and inclination control
10 °	30.36 ± 3.74	25.0 ± 2.0
20 °	301.9 ± 148.35	45.0 ± 8.77
30 °	not possible	156.5 ± 39.56

adapted foot tip positions and it estimates the changing terrain characteristics. In segment A of the multi-terrain testbed, it can be seen that the position controller's CoT (blue line) begins to increase towards infinity as its speed approaches zero whereas using impedance and inclination control (black line), the CoT only increases a finite amount. The impedance and inclination controller reduces the CoT by an average of $54.3\,\%$ in segment A. With position control (blue line) the robot gets stuck due to the increasing roughness and inclination of the terrain in segment A. After repositioning Weaver with the position controller (red line) in segment B of the multi-terrain testbed, Weaver gets stuck again in segment D and some of the actuators reach their torque limits. The impedance and inclination controller (black line) enables Weaver to traverse this challenging terrain. Moving stones cause a sudden change of the velocity in segment D and for a few runs with the impedance and inclination controller (black line) this causes a drop in velocity and consequently, a high CoT. The robot copes with the changing terrain conditions and continues the run. This also explains the high standard deviation around the peaks. The experiment was not repeated for Weaver with only position control since it became apparent that the controller was not able to cope with the terrain and a repetition could damage the robot. The percentage reduction of variance (23) is calculated with

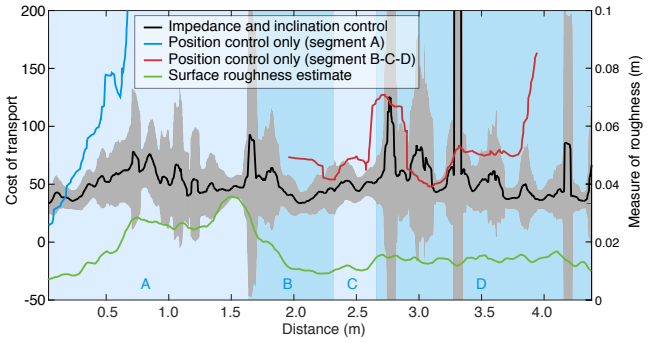

Fig. 12. Results of the multi-terrain experiment show the CoT of the position controller and the impedance controller. The adapted foot tip positions of the impedance and inclination controller estimate the roughness of the terrain by calculating the center line average. The black colored line is the mean and the grey shading is one standard deviation of the impedance and inclination controller.

one run of the position controller and all 15 runs of the impedance and inclination controller. $S_{roll} = 58.51\,\%$ and $S_{pitch} = 63.66\,\%$ are the results of segment A and $S_{roll} = 88.01\,\%$ and $S_{pitch} = 73.86\,\%$ are the results of segment B-C-D. The phase planes of the pitch and roll movement for two runs in Fig. 13 confirm the self-stabilizing effect of the impedance controller. The angular body movements of the position controller (red line) are reaching unstable limit cycles. The impedance and inclination controller (blue line) reduces this effect and the limit cycles stay closer around zero angle and zero angular velocity.

V. DISCUSSION

The experimental results successfully demonstrated the ability of Weaver to overcome challenging terrain without prior profiling of the terrain with exteroceptive sensors and complex planning algorithms. The results of the multi-terrain testbed reveals that the impedance controller enables the robot to adapt to uneven terrain. This effectively decreases the CoT and distinctly increases the stability of the robot by reducing the body movement. A spin-off of the impedance controller is the possibility to estimate the roughness of the terrain due to the different foot placements. The roughness estimation is not strictly required to perform locomotion. However, it evaluates the performance of the controller and it also confirms the adaptive approach of the foot tip position due to uneven terrain. In addition, the versatile controller design accommodates different leg configurations without

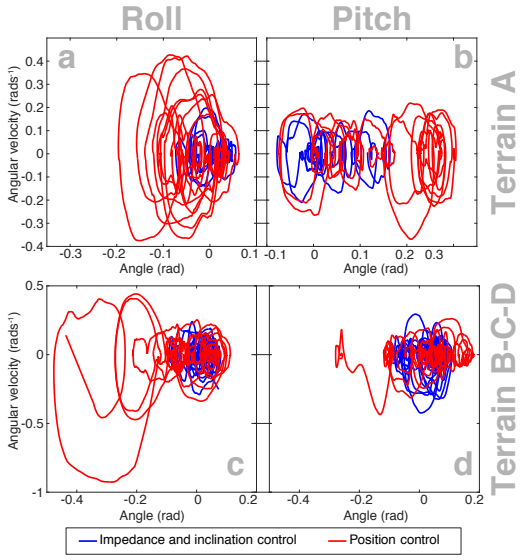

Fig. 13. Limit cycles of the roll and pitch movement projected onto the phase plane for different segments of the multi-terrain testbed.

the need for inverse dynamics. The result on flat terrain also shows the limitations of the controller in its current implementation. The same elastic configuration of the legs used on the multi-terrain testbed slightly increases the CoT on flat terrain. This indicates a high stiffness setting is desirable for flat hard terrain while a low stiffness is desirable for uneven or soft terrain. The inclination controller in combination with the inverse kinematics improves the locomotion of Weaver on slopes and extends the field of applications to terrains with higher slopes. By comparison: LAURON V walks up inclinations up to 25 °and remains stable until 42.8 ° [21]. The results show that Weaver is increasing the maximum angle for the dynamic and static case to 30 °and 50 °. A comparison between LAURON V and Weaver is only conditionally possible because the highest inclination angle depends on the friction of the contact surface. The multi-terrain testbed also verifies the integration of the impedance and inclination controller into the hierarchical controller. Weaver copes with high inclination gradients in any direction with respect to the body and uneven terrain.

VI. CONCLUSIONS

This work introduced Weaver, the 30 DoF hexapod and proposed a hierarchical controller that extends the field of application of the robot. The reactive impedance and inclination controller adapt the legs' position and orientation to improve locomotion based on proprioceptive sensing. Weaver traverses challenging terrain and high gradient slopes in any direction relative to the body frame. The paper focused on reactive locomotion without implementing complex planning algorithms based on exteroceptive sensing. The proposed controllers were evaluated on a real robot and the results were presented showing its effectiveness. The results from the flat terrain experiment show the utility of using adaptive parameters instead of constant parameters in the impedance controller. In future work, parameter adaptation with respect to the roughness of the ground will be investigated to improve locomotion of varying terrain. It is possible to use information from the roughness estimation of the foot tip positions to adapt these parameters. In conclusion, this work demonstrated that the robot's low-level autonomy enables it to explore rough terrain environments.

ACKNOWLEDGMENTS

The authors would like to thank Ryan Steindl, Thomas Lowe, Yufei Jiang, Brett Wood and John Whitham for their support during the project.

REFERENCES

[1] J. E. Bares and W. L. Whittaker, "Configuration of autonomous walkers for extreme terrain," *The International Journal of Robotics Research*, vol. 12, no. 6, pp. 535–559, 1993.

[2] R. Siegwart, I. R. Nourbakhsh, and D. Scaramuzza, "Locomotion," in *Introduction to autonomous mobile robots*. MIT press, 2011, pp. 13–38.

[3] S. Kajita and B. Espiau, "Legged robots," in *Springer Handbook of Robotics*, B. Siciliano and O. Khatib, Eds. Springer Berlin Heidelberg, 2008, pp. 361–389.

[4] D. Messuri and C. Klein, "Automatic body regulation for maintaining stability of a legged vehicle during rough-terrain locomotion," *IEEE Journal of Robotics and Automation*, vol. 1, no. 3, pp. 132–141, 1985.

[5] J. Estremera and K. J. Waldron, "Thrust control, stabilization and energetics of a quadruped running robot," *The International Journal of Robotics Research*, vol. 27, no. 10, pp. 1135–1151, 2008.

[6] R. Blickhan, "The spring-mass model for running and hopping," *Journal of biomechanics*, vol. 22, no. 11, pp. 1217–1227, 1989.

[7] R. Full and D. Koditschek, "Templates and anchors: neuromechanical hypotheses of legged locomotion on land," *Journal of Experimental Biology*, vol. 202, no. 23, pp. 3325–3332, 1999.

[8] D. J. Hyun, S. Seok, J. Lee, and S. Kim, "High speed trot-running: Implementation of a hierarchical controller using proprioceptive impedance control on the MIT Cheetah," *The International Journal of Robotics Research*, vol. 33, no. 11, pp. 1417–1445, 2014.

[9] A. De Luca and W. Book, "Robots with flexible elements," in *Springer Handbook of Robotics*, B. Siciliano and O. Khatib, Eds. Springer, 2008, pp. 287–319.

[10] K. Nonami, R. K. Barai, A. Irawan, and M. R. Daud, "Force-based locomotion control of hexapod robot," in *Hydraulically Actuated Hexapod Robots*. Springer, 2013, pp. 141–167.

[11] D. Belter and K. Walas, "A compact walking robot flexible research and development platform," in *Recent Advances in Automation, Robotics and Measuring Techniques*, ser. Advances in Intelligent Systems and Computing, R. Szewczyk, C. Zieliński, and M. Kaliczyńska, Eds. Springer, 2014, vol. 267, pp. 343–352.

[12] D. Goldschmidt, F. Hesse, F. Worgotter, and P. Manoonpong, "Biologically inspired reactive climbing behavior of hexapod robots," in *IEEE/RSJ International Conference on Intelligent Robots and Systems (IROS)*, 2012, pp. 4632–4637.

[13] M. Görner, T. Wimböck, A. Baumann, M. Fuchs, T. Bahls, M. Grebenstein, C. Borst, J. Butterfass, and G. Hirzinger, "The DLR-Crawler: A testbed for actively compliant hexapod walking based on the fingers of DLR-Hand II," in *IEEE/RSJ International Conference on Intelligent Robots and Systems (IROS)*, 2008, pp. 1525–1531.

[14] W. A. Lewinger, H. M. Reekie, and B. Webb, "A hexapod robot modeled on the stick insect, *Carausius morosus*," in *International Conference on Advanced Robotics (ICAR)*, 2011, pp. 541–548.

[15] A. Roennau, G. Heppner, M. Nowicki, and R. Dillmann, "LAURON V: A versatile six-legged walking robot with advanced maneuverability," in *IEEE/ASME International Conference on Advanced Intelligent Mechatronics (AIM)*, 2014, pp. 82–87.

[16] K. Inoue, T. Tsurutani, T. Takubo, and T. Arai, "Omni-directional gait of limb mechanism robot hanging from grid-like structure," in *IEEE/RSJ International Conference on Intelligent Robots and Systems (IROS)*, 2006, pp. 1732–1737.

[17] A. Roennau, T. Kerscher, and R. Dillmann, "Design and kinematics of a biologically-inspired leg for a six-legged walking machine," in *IEEE International Conference on Biomedical Robotics and Biomechatronics (BioRob)*, 2010, pp. 626–631.

[18] N. Kottege, C. Parkinson, P. Moghadam, A. Elfes, and S. P. Singh, "Energetics-informed hexapod gait transitions across terrains," in *IEEE International Conference on Robotics and Automation (ICRA)*, 2015.

[19] J. Nishii, "Legged insects select the optimal locomotor pattern based on the energetic cost," *Biological Cybernetics*, vol. 83, no. 5, pp. 435–442, 2000.

[20] S. Hirose, H. Tsukagoshi, and K. Yoneda, "Normalized energy stability margin and its contour of walking vehicles on rough terrain," in *IEEE International Conference on Robotics and Automation (ICRA)*, vol. 1, 2001, pp. 181–186.

[21] A. Roennau, G. Heppner, M. Nowicki, J. Zoellner, and R. Dillmann, "Reactive posture behaviors for stable legged locomotion over steep inclines and large obstacles," in *IEEE/RSJ International Conference on Intelligent Robots and Systems (IROS)*, 2014, pp. 4888–4894.

[22] L. Villani and J. De Schutter, "Force control," in *Springer Handbook of Robotics*, B. Siciliano and O. Khatib, Eds. Springer Berlin Heidelberg, 2008, pp. 161–185.

[23] J. Nishii, "An analytical estimation of the energy cost for legged locomotion," *Journal of Theoretical Biology*, vol. 238, no. 3, pp. 636 – 645, 2006.

[24] T. Perez, "Ship motion performance," in *Ship Motion Control*, ser. Advances in Industrial Control. Springer London, 2005, pp. 127–142.

[25] R. Hoffman and E. Krotkov, "Terrain roughness measurement from elevation maps," in *SPIE Vol 1195 Mobile Robols IV*, 1989.